Optics & Laser Technology 160 (2023) 109052

Contents lists available at ScienceDirect

Optics and Laser Technology

journal homepage: www.elsevier.com/locate/optlastec

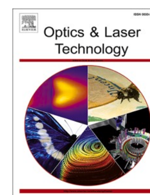

Full length article

An individual ZnO microwire homojunction LED with ultraviolet electroluminescence spectrally purified using Pt nanoparticles cladding

Dailong Wang [a], Maosheng Liu [a], Shenao Shang [a], Peng Wan [a], Daning Shi [a], Caixia Kan [a], Binghui Li [b,*], Mingming Jiang [a,*]

[a] College of Physics, MIIT Key Laboratory of Aerospace Information Materials and Physics, Key Laboratory for Intelligent Nano Materials and Devices, Nanjing University of Aeronautics and Astronautics, No. 29 Jiangjun Road, Nanjing 211106, PR China

[b] State Key Laboratory of Luminescence and Applications, Changchun Institute of Optics Fine Mechanics and Physics, Chinese Academy of Sciences, Changchun 130033, China

ARTICLE INFO

Keywords:
homojunction LED
ZnO:Sb microwires
P-type conductivity
Pure ultraviolet
Pt nanoparticles
Ultraviolet plasmons

ABSTRACT

Low-dimensional ultraviolet light sources are enormous significance due to their wide range of potential applications, ranging from bioscience and high-resolution biological imaging, environmental conservation to public hygiene. Nevertheless, developing energy-efficient and cost-efficient light sources still remains serious challenges. In this study, p-type ZnO microwires with Sb-incorporation (ZnO:Sb MWs) were synthesized individually. The p-type conductivity was proofed using an individual MW based back-gated field-effect transistor; while the ZnO:Sb MWs with quadrilateral cross-section exhibited stimulated emission resonant in well-defined Fabry-Perot mode on the benefit of single-crystalline quality and atomically smooth side facets. The newly synthesized ZnO:Sb MW was further used to fabricate homojunction light-emitting device by employing *n*-type ZnO film as electron-transporting layer. A strong ultraviolet emissions peaking at around 378.5 nm was achieved upon forward biased electrically, but illustrating much broader electroluminescence (EL) linewidth. Introducing Pt nanoparticles (PtNPs) with desired plasmons, the light-out intensity is significantly enhanced. Particularly, the broad EL profiles narrowed to about 16.6 nm at high injection regime, achieving electron-holes radiative recombination in the ZnO:Sb MWs active region. The results exhibit a prominent progress achieving high-quality ZnO nano/microstructures with genuine p-type conductivity, which has great hopes for its future applications and development in ZnO homojunction optoelectronic devices.

1. Introduction

Ultraviolet electromagnetic radiation, proverbially regarded as ultraviolet light sources, is currently employed in many industries and applications, such as biological/chemical sensing, detection, medical treatment, material processing, disinfection with the recent COVID-19 pandemic and so on [1–7]. The emerging ultraviolet light-emitting diodes (LEDs) and laser diodes (LDs), which have been constructed based on wide-bandgap semiconductors, will be an enabling, competitive technology that drives new and innovative applications. The light sources of LEDs and LDs have a longer operating life, and are much more green, energy saving and environmental protection than traditional mercury ultraviolet lamps [8,9,10,11,12]. At present, the mature ultraviolet light sources are mostly fabricated on account of GaN-based materials, structures and devices [13–15]. With the tremendous advances of nanoscience and nanotechnology, low-dimensional materials as building blocks for ultraviolet light sources have attracted intense attentions, indicating their promising potential applications in integrated photonics devices and systems. In contrast to traditional LEDs and LDs that have been constructed based on thin-film and bulk structures, the nanostructured ones have higher efficiency, much more compact and smaller size, and lower power-consumption. Those are largely due to the interior of nanostructures, which currently exhibiting natively self-constructed microcavities, defect-free, excellent laser gain characteristics, high-crystalline quality and so on [16–20]. Success in developing compact ultraviolet LEDs and LDs has been extremely limited due to time-consuming, high-cost, complicated fabrication and/or growth process. Despite the overall progress of GaN-based microLED displays, such as epitaxial growth approach, nanoimprint lithography, etching technique, many peculiarities of these materials, structures and

* Corresponding authors.
E-mail addresses: binghuili@163.com (B. Li), mmjiang@nuaa.edu.cn (M. Jiang).

https://doi.org/10.1016/j.optlastec.2022.109052
Received 14 November 2022; Received in revised form 14 December 2022; Accepted 17 December 2022
Available online 29 December 2022
0030-3992/© 2022 Elsevier Ltd. All rights reserved.

devices still face intractable problems, especially for the springhead of the decline of LED efficiency, which are produced by various loss mechanisms of joule heating, leakage current and nonradiative recombination in the course of the carrier transport and carrier recombination procedure [13,15,21,22,23].

Progress in this field, with a broad gap energy of 3.37 eV and a large exciton binding energy ~60 meV at room temperature, ZnO has acquired extensive concerns as a potential semiconductor to develop ultraviolet optoelectronic devices, containing high-brightness LEDs, low-threshold LDs, photodetectors and sensors in the ultraviolet region [4,11,24,25,26,27,28]. Particularly, low-dimensional ZnO via single-crystalline nature averagely has a wurtzite structure and exhibits a naturally-formed geometries, which currently serves as good gain media and optical cavities. Inspired by its unique geometries and atomically smooth side facets, many attempts have been devoted to exploit ZnO-based micro- and nanolasers, containing Fabry-Perot (FP) mode, random mode, Whispering Gallery Mode (WGM) and so on [29–34]. Nevertheless, the high-quality single-crystalline p-type ZnO is still a bottleneck and focused area of frontier research, which hinders the development of ZnO optoelectronic devices, although various preparation technologies of p-type ZnO with different dopants have been reported previously [8,26,27,35]. Among those doping elements, Sb has been regarded as a highly promising candidate to synthesize p-type ZnO even if its atomic size is much larger [11,36,37,38,39]. Theoretically predicted that, because of large-size-mismatched impurity to Sb doping, p-type ZnO could be evidenced using first–principle via Sb_{Zn}-$2V_{Zn}$ complexes model [40]. Experimentally, Sb has been proven to be a good p-type dopant for ZnO nanostructures, and the p-type ZnO:Sb nanostructures has evidently provided as ideal systems to construct homojunction LEDs and laser devices by combining *n*-type ZnO substrate [41–46]. Nevertheless, the achievement of ZnO homojunction LEDs with high-brightness, and LDs with distinguishable lasing modes, has not yet implemented, severely limiting their practical applications.

In this research, we synthesized single-crystalline p-type ZnO microwires via Sb-doped (ZnO:Sb MWs) using a facile chemical vapor deposition (CVD). The p-type conductivity of ZnO:Sb MWs was researched using a single-wire field-effect transistor (FET), confirming its hole conduction channel. Subsequently, optical pumping measurement made on a ZnO:Sb MW exhibited that the quadrilateral structures can function as optical cavity, supporting FP lasing. Employing as promising ultraviolet electroluminescent materials, a single ZnO:Sb MW was utilized to construct homojunction LED with *n*-type ZnO film, showing an excellent rectifying property with a threshold voltage of approximately 3.25 V and strong ultraviolet emission peaking at 378.5 nm. However, the LED revealed much broader electroluminescence (EL) linewidths ~40 nm. Benefit from Pt nanoparticles (PtNPs) coating with appropriate sizes, the ultraviolet EL emission was significantly increased, accompanying by a significant reduction of their linewidths to about 16.6 nm. Therefore, typically ZnO:Sb band-edge emission was achieved in the single MW active media in the as-constructed p-PtNPs@ZnO:Sb MW/*n*-ZnO homojunction. The achievement of relatively pure ultraviolet EL induced by cladding PtNPs was studied in detail, which was due to the excitation of Pt plasmons. We anticipate that this study will inspire more experimental attempts on the preparation of reliable p-type ZnO, as well as the development of ZnO homojunction optoelectronic devices.

2. Experimental section

2.1. Sample preparation

Highly-purified antimony oxide (Sb_2O_3) powder was utilized as p-type impurity dopant source to achieve the preparation of individual Sb-doped ZnO microwires (ZnO:Sb MWs) [33,36,47]. The synthesis of ZnO-based nano- and microstructures was carried out using a simple CVD method, and the experimental scheme was performed in a simple tube furnace via double high temperature zones. The precursor mixture contains ZnO, Sb_2O_3 and carbon powders with a weight ratio of 9:1:10. The thoroughly mixed precursor was contained in a corundum boat, and a Si chip was put on the top surface of the source materials. The boat was positioned at the heating area in the furnace. A carrying gas of 120 sccm Ar and 5 sccm O_2 was imported into the quartz tube as protecting gas and an oxygen source, respectively. In the synthesis regime, the temperature at the heating zone was heated to about 1100 °C at a rate of 25 °C/min. The sample preparation was carried out for about 1 h under normal ambient pressure. As the growth was accomplished, the temperature of the depositing region dropped to room temperature slowly. The sample of individual ZnO:Sb wires were acquired around Si substrate. The as-synthesized ZnO:Sb MWs on the length scales vary from submillimeter to centimeter, while the cross-sectional diameter varies from hundreds nanometers to dozens of micron range.

2.2. Device fabrication

Fabrication of a single wire FET: A single ZnO:Sb wire based FET device was constructed [27,37,45]. The heavily-doped Si chip covered by 200 nm thick SiO_2 was utilized as the device substrate. An individual ZnO:Sb wire was mechanically placed on the SiO_2/Si substrate. Au particles were welded on both ends of the ZnO:Sb MW by using FIB-SEM system. Thus, a single ZnO:Sb MW FET device was fabricated.

Preparation of PtNPs: Pt quasiparticle films were evaporated on a clean sapphire substrate (dual-face polishing) using electron beam thermal evaporation method. The evaporation of Pt film with controlled thickness was carried out at a speed of 0.02 nm/s under a constant pressure of 7.5×10^4 Pa. An annealing treatment was carried out in a N_2 atmosphere at 600 °C. Maintaining about 30 min, a layer of PtNPs with relatively uniform sizes could be yielded on the sapphire substrate. The preparation of PtNPs with changeable sizes, such as the diameter and gap distances, could be realized [26,48,49,50].

Fabrication of a PtNPs@ZnO:Sb MW: An individual ZnO:Sb MW was mechanically transferred on a clean quartz substrate. Ag pastes were used as electrodes to immobilize the wire on the substrate, forming an Ag-ZnO:Sb-Ag (MSM) structured incandescent-type light bulb. Highly-purified Pt was evaporated onto the ZnO:Sb MW using electron beam thermal evaporation method, yielding a thin film covered the wire. Thus, an individual ZnO:Sb MW covered by a layer of Pt nanofilm (Pt@ZnO:Sb) was fabricated. When biased electrically, the fabricated single wire MSM incandescent-type light bulb channel began to emit visible light at its centre, and its brightness and area of light-emission increase with an increase of the applied bias voltage. The brightest region of the light-emission is positioned at the centre of the ZnO:Sb wire, which coincides with the location of the largest temperature zone. The pre-evaporated Pt nanofilms in the center of ZnO:Sb MW were melted into discrete nanoparticles because of Joule heating effect. In brief, a hybrid structure involving an individual ZnO:Sb MW covered by PtNPs (PtNPs@ZnO:Sb) was created. Particularly, PtNPs with different sizes would be capable of preparing on the MW by changing the evaporation time of Pt nanofilms [26,49,50].

Fabrication of Homojunction LED: One-dimensional wirelike ZnO homojunction LED light source featuring in the ultraviolet region, which is consisting of a p-type ZnO:Sb MW and *n*-type ZnO film, was proposed and fabricated. The LED fabrication procedure is as follows [26,51]. First, a 200 nm thick ZnO film was grown on sapphire substrate in a molecular beam epitaxy (MBE) system equipped with oxford radio-frequency (RF) atom sources. Second, an Au film with 100 nm in thickness used for the *n*-type contact was deposited on *n*-type ZnO film using electron beam heating evaporation. Third, a 100 nm thick MgO film was evaporated on the other side of ZnO film using electron beam evaporation. Fourth, a single ZnO:Sb MW was mechanically placed on ZnO film. One segment of the wire was laid on the MgO layer. Finally, with the aid of a mask, Au film was evaporated on the segment of the ZnO:Sb MW, which has been laid on the MgO layer. In the as-designed

LED structure, Au films employing as the ohmic contact electrodes for the current injection of the as-designed p-ZnO:Sb MW/*n*-ZnO homojunction LE. Similarly, the single ZnO:Sb MW covered by PtNPs was further used to construct homojunction LED, as we described above.

2.3. Characterizations

Optical characterization of the CVD-prepared ZnO:Sb MW uncovered and covered by PtNPs, and ZnO film were examined using a photoluminescence (PL) system. The PL measurement system contains a 325 nm He-Cd laser as excitation light source, a high-resolution LabRAM-UV Jobin-Yvon spectrometer and a high-sensitivity charge-coupled device (CCD). Lasing characterization of a single ZnO:Sb MW was tested using a 355 nm femtosecond (fs) laser (pulse duration of 150 fs, repetition rate of 1000 Hz). The excitation laser beam was focused on the wire body by a microscope objective. The light output was recorded using an optical multichannel analyzer (Princeton, Acton SP2500i). Electrical characterizations of a single ZnO:Sb MW without and with PtNPs covering, ZnO film, the fabricated single ZnO:Sb wire FET device and the fabricated ZnO:Sb MW homojunction LEDs were tested using a sourcemeter system. EL characterizations of the as-fabricated LEDs were checked using the high-resolution LabRAM-UV Jobin-Yvon spectrometer and a high-sensitivity charge-coupled device (CCD). EL photographs were captured using a CCD camera. In the EL research, a direct and continuous current power source was employed to bias the LEDs electrically.

2.4. Theoretical calculation

Three-dimensional model involving a semispherical Pt nanostructure was built up, and a hybrid structure which is made of the semispherical Pt nanostructure placed on ZnO:Sb MW was further constructed. The electric field distributions of the metal nanoparticle was simulated using a finite-differential time-domain simulation method. The spatial localization and distribution of electric-field intensities of the nanostructured Pt, can be simulated respectively. The refractive indexes of ZnO:Sb ($n_{ZnO:Sb}$), air (n_{air}) are 2.35 and 1.0, respectively. In the simulation regime, the plane wave outgoing the targets were perfectly absorbed by surrounding perfect matched layer (PML); while the wavelength of incident light λ is referred to the value, which was observed according to the strongest extinction peak experimentally (See Fig. 4 (a)). The size of PtNP, especially for its diameter, was characterized to approximately 80 nm. The complex relative permittivity of Pt at λ = 365 nm is evaluated to about$\varepsilon_{Pt} = n + ik = 0.85 + 2.76\,i$.

3. Results and discussions

As previously reported, Sb as an efficient dopant has been regarded as highly promising candidate to achieve p-type ZnO theoretically and experimentally. The electronic transport characteristic was evidenced to be p-type using first-principle. In the theoretical model, the Sb_{Zn}-$2V_{Zn}$ complexes can feature as acceptor source [11,36,40]. In this study, individual p-type ZnO:Sb wires were successfully prepared using highly-purified Sb_2O_3 powder as the doping source. In the Experimental Section, the preparation method can give ZnO:Sb wires with high yield, size controllability, and repeatability. Scanning electron microscopy (SEM) graph of single ZnO:Sb wire was exhibited in Fig. 1(a). Illustration in the figure, the typical single ZnO:Sb MW exhibits high morphological quality that showing regular quadrilateral shape, smooth sidewall facets and sharp edges. The cross-section of the well-defined quadrilateral ZnO:Sb MW is shown in the inset of Fig. 1(a). The Energy-dispersive-spectroscopy (EDS) analysis of the as-synthesized ZnO:Sb samples was performed, with the corresponding elemental constituents is demonstrated in Fig. 1(b). Clearly, the species that containing Zn, Sb and O are presented in a single ZnO:Sb wire. Thus, the EDS elemental mapping

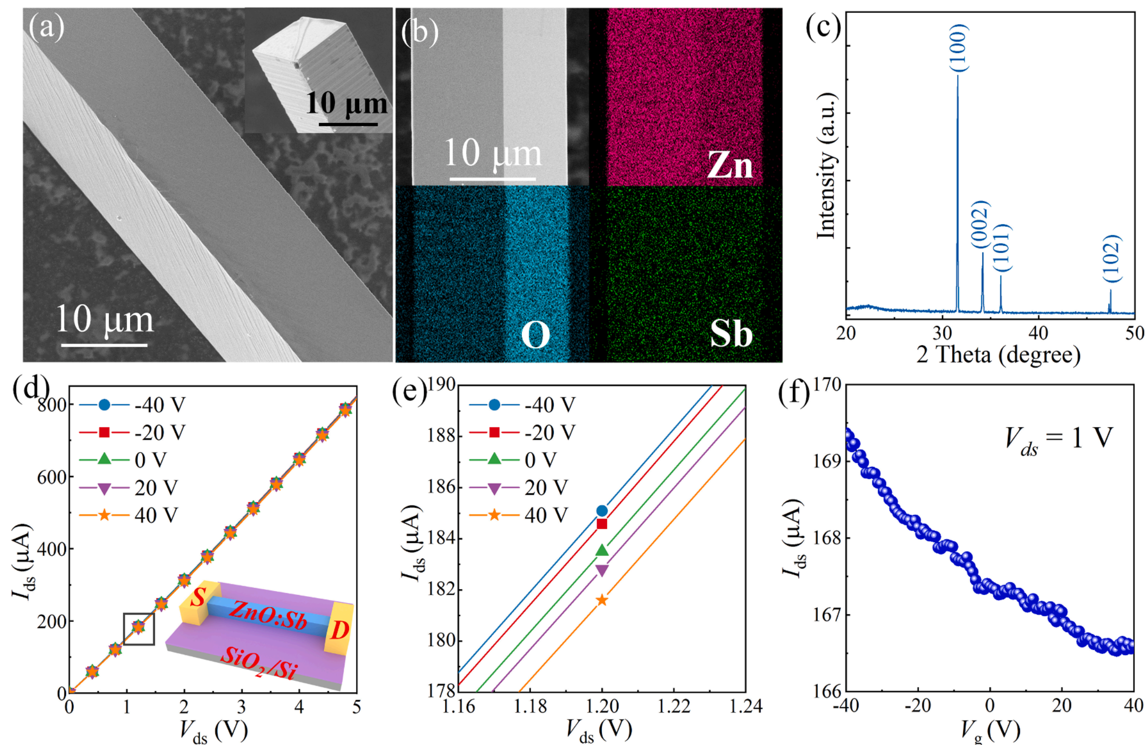

Fig. 1. Characterization of CVD-obtained ZnO:Sb samples. (a) A typical SEM observation of a single ZnO:Sb wire. Inset: The enlarged tilt view of a single ZnO:Sb MW, demonstrating a quadrilateral cross-section, smooth end and side facets. (b) SEM image and elemental compositions of a single ZnO:Sb wire, showing uniform distribution of Zn, Sb and O species. (c) XRD pattern of CVD-synthesized ZnO:Sb wires. Electrical properties of an individual ZnO:Sb MW FET, (d) I_{ds}-V_{ds} curves at different back-gate voltages, and the inset shows a schematic view of as-designed ZnO:Sb MW FET structure; (e) An enlarged I_{ds}-V_{ds} curves marked in (d); (f) I_{ds}-V_g characteristic curves of the fabricated ZnO:Sb MW FET at $V_{ds} = 1$ V.

results suggest that the incorporated Sb atoms were uniformly incorporated into the ZnO crystal lattice [11,37,47]. X-ray diffraction (XRD) pattern measurement of the as-synthesized ZnO:Sb samples was performed. The measured XRD pattern in Fig. 1(c) exhibits that three strong peaks at 31.6°, 34.1° and 36.0° are belong to ZnO (1 0 0), (0 0 2), and (1 0 1) crystal planes, respectively; while no other peaks could be observed. The result suggests that the CVD-grown ZnO:Sb MWs are single crystal property via *c*-axis oriented [11,25,37,47]. Conclusively, the CVD-synthesized ZnO:Sb MWs with high crystal quality were obtained by one-step CVD method.

The electronic transport properties of an individual ZnO:Sb wire was researched using a back-gate FET structure. The schematic illustration of a single wire based FET device structure is represented in the inset of Fig. 1(d). In the FET structure, a 200 nm film of SiO_2 was prepared on Si substrate, thus, the SiO_2/Si substrate was employed as the back-gate and dielectric gate oxide. The gap distance between source and drain electrodes (Au) was measured to approximately 50 μm. When operated under various gate voltages, the measured I_{ds}-V_{ds} curves of drain current versus drain source voltage of the as-constructed single ZnO:Sb wire FET device was exhibited in Fig. 1(d). Enlarged I_{ds}-V_{ds} curves measured at $V_{ds} = 1.20$ V was illustrated in Fig. 1(e). It is obviously presented that as the gate voltage V_g is reduced from 40 to −40 V, the tendency of the curve becomes sharper. The dependence of I_{ds} on the gate voltage V_g was measured at a $V_{ds} = 1.0$ V. Accordingly, the relationship of I_{ds}-V_g is plotted in Fig. 1(f). As the V_g varying from −40 to 40 V, the I_{ds} is observably reduced, thus suggesting the hole conduction channels. It is apparent that the CVD-synthesized individual ZnO:Sb MWs have p-type semiconductor conductivity characteristics [27,35,37].

The single crystalline quality of the CVD-prepared individual ZnO:Sb MWs would give rise to excellent optical properties and lasing actions. The exciton binding energy ~ 60 meV could facilitate a prominent excitonic influence at room temperature, rendering the as-synthesized ZnO:Sb samples much more efficient light emitters and gain medium for stimulated emissions [11,26,33]. Indeed, the lasing action could be realized in single ZnO:Sb wire when pumped optically by a 355 nm fs laser. In the optical pumping, the laser spot can cover the cross-sectional diameter of CVD-prepared ZnO:Sb MWs. Fig. 2(a) exhibits optical micrograph of ZnO:Sb wire luminescence at a high excitation fluence ~ 145.6 μJ/cm². From the emission image, the large fluence can result in localized regions of enhanced light-emitting region, which distributed along the bilateral facets of the ZnO:Sb MW. Varying the excitation fluence, the emitted photons were recorded. Fig. 2(b) reveals the PL spectra at excitation fluences of 34.8, 56.5 and 71.2 μJ/cm², respectively. The PL spectra exhibit an approximately linear feature: at low excitation power density of 34.8 μJ/cm², a broad spontaneous radiation peaking at around 390.0 nm and line width of about 17.5 nm dominates the PL spectrum. With an increase of the excitation fluence up to 71.2 μJ/cm², a series of two sharp peaks at the longer wavelength shoulder of PL spectra was observed. Further, Fig. 2(c) displays PL spectra in terms of excitation fluence ranging from 34.8 to 145.6 μJ/cm². With increasing excitation power fluence that exceeding 78.8 μJ/cm², a group of narrow PL lines, which are resolved from the broad PL spectra, appear. These sharp PL subpeaks grow superlinearly in their intensities with an increase of excitation power fluence, marking the occurrence of stimulated radiation. Eventually, these sharp lines occupy over the whole PL spectra, thus yielding a hallmark of lasing radiation [29,33,49].

As previous studies published, low-dimensional semiconductors with

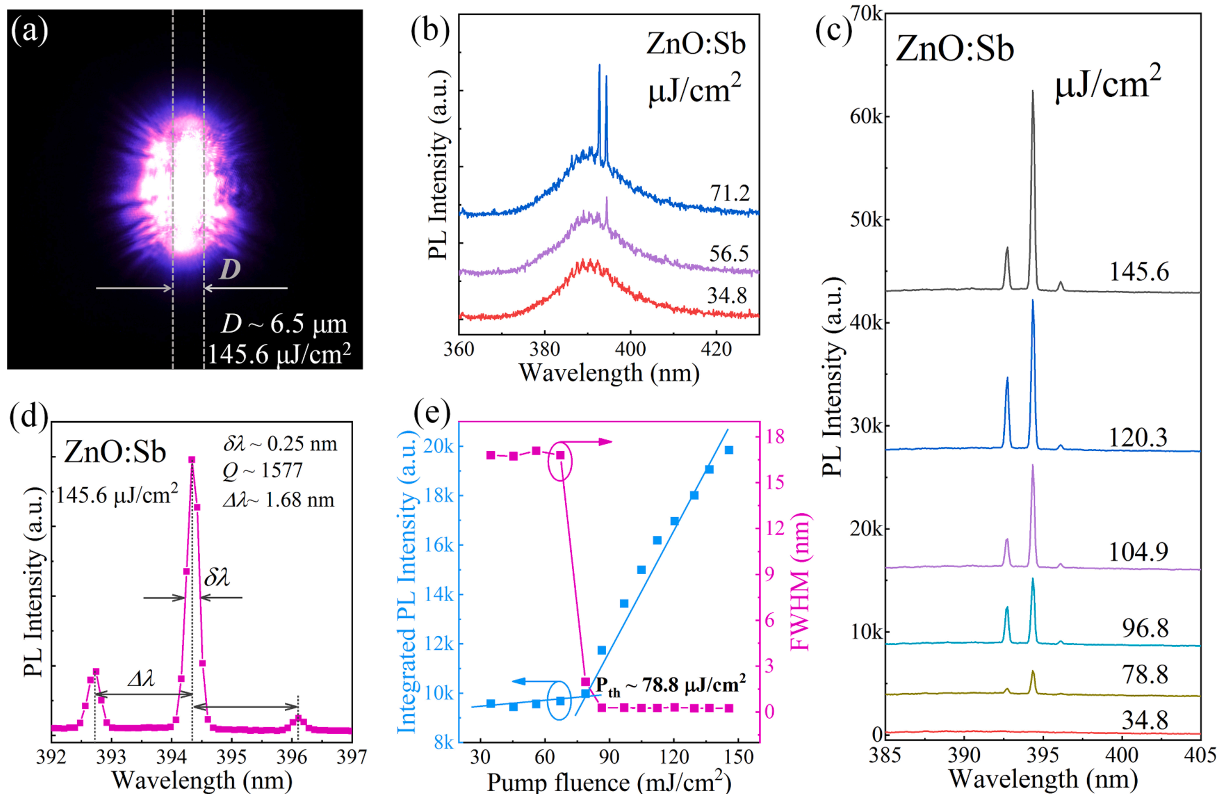

Fig. 2. Lasing characterization of a ZnO:Sb MW under the laser excitation at a wavelength of 355 nm. (a) A far-field PL image of ZnO:Sb MW emission pumped at an excitation fluence of 145.6 μJ/cm². (b) The plot of PL spectra by changing the pumping fluence from 34.8 to 71.2 μJ/cm². (c) The evolution varying from the spontaneous radiation to lasing with an increase of pumping fluence. From down to up, sharp lasing peaks appear, and then dominate the PL spectra as the excitation intensity increasing above the laser threshold. (d) A magnified view of a PL spectrum when pumped at an excitation power intensity of 145.6 μJ/cm², yielding a Q-factor value of about 1577. (e) Representative dependencies of integrated PL intensity and FWHM of the main lasing peaks on the excitation power intensity, giving rise to the threshold fluence of 78.8 μJ/cm².

rectangular-shaped cross section have been widely used to construct lateral-cavity FP microlasers because of single crystal property and smooth facets. The sample of ZnO nano- and microstructures, such as nanowires, microribbons, microwires with quadrilateral cross section, has been extensively applied to fabricate FP microlaser devices [31–33]. The observed multimode emission features of a quadrilateral ZnO:Sb MW were investigated. Despite the pumping fluence, the obtained PL features, which contain the peak distances between neighboring resonant modes, the line width of the predominant emission peak and the emission center, are seemingly unchanged. It is particularly important that the line widths of the main emission modes remain unchanged at elevated pumping fluences. Taken a PL spectrum pumped at an excitation fluence of 145.6 μJ/cm^2 for example, the full width at half maximum (FWHM) of the main lasing mode is measured to about $\Delta\lambda \sim 0.25$ nm; while the equably spaced gap ($\Delta\lambda$) of PL spectra with multi-peak modes is measured to approximately 1.68 nm (See Fig. 2(d)). The Q-factor corresponding to the observed FWHM of the main lasing peak was calculated to ∼ 1577 according to the equation $Q = \lambda/\Delta\lambda$, in which λ is the luminescence wavelength. Theoretically, the understanding on the PL characteristics of the quadrilateral ZnO:Sb wire was examined. The spaced gap for typical FP microcavity is derived as follows [31,33,52]:

$$\Delta\lambda = \frac{\lambda^2}{2L_c\left(n - \lambda\frac{dn}{d\lambda}\right)} \quad (1)$$

In which, the cavity length L_c is the width of the used quadrilateral ZnO:Sb wire, $dn/d\lambda$ is evaluated to about -0.010 nm^{-1} at 390 nm. Thus, L_c is calculated to about 6.5 μm, which is approximatively comparable to the value of experimental observation. Therefore, the sample of individual ZnO:Sb nano/microcrystals with quadrilateral morphologies and straight facets can enable to construct FP microresonators. Fig. 2(e) exhibits the variations of integrated PL intensity and the FWHM in terms of excitation fluence, respectively. The course of evolution for the obtained PL spectra demonstrates an instantaneous sharp decreasing in FWHM and an abrupt change for light input–output around the laser threshold. The distinct narrowing of FWHM and superlinear increase of PL intensity above the $P_{th} \sim 78.8$ μJ/cm^2, confirm the occurrence of FP lasing action.

Previous research has found that, one-dimensional ZnO wire-like structures, which were doped by Ga, Al and Sb dopants, have been widely used to fabricate incandescent-type filament bulb [26,47,49,53]. Considering the high crystal quality and preeminent transport properties of charge carriers, an individual ZnO:Sb MW was employed to construct MSM-type structure device, in which Ag pastes were utilized as the electrodes. When biased electrically, the single wire can emit bright green light, and the resulting luminescence photograph was exhibited in Fig. 3 (a). Cladding Pt nanofilms on the wire (the evaporation time ∼ 350 s), EL characteristics of the as-constructed single ZnO:Sb MW-based filament bulb, such as the light wavelengths and emitting color, were changed greatly. Accordingly, the luminescence photographs were further filmed in Fig. 3(b). The modulation of the Pt nanostructures on the EL characterization of an individual ZnO:Sb MW MSM light source was studied [26,49,50]. After being biased electrically, the morphologies of the coating were examined. First, Fig. 3(c) exhibits SEM image of Pt nanofilm, which has been evaporated on the ZnO:Sb wire. The region ∼ **I** is associated with nonlighting region in the Pt@ZnO:Sb wire, showing quasi-particle film. That is, there is no significant change of the evaporated Pt nanofilms in the non-luminescence regions. Second, the segment of the sample positioned toward the critical area between electroluminescent and non-electroluminescent regions was examined. The SEM figure in region-**II** is represented in Fig. 3(d). Notably, a marked difference varying from quasi-particles film to physically isolated nanoparticle is observed. Finally, Fig. 3(e) shows the SEM graph of wire, which is positioned at the electroluminescent region (∼**III**). It is notably illustrated that uniform distribution of discrete PtNPs have been formed on the ZnO:Sb MWs [26,49,54].

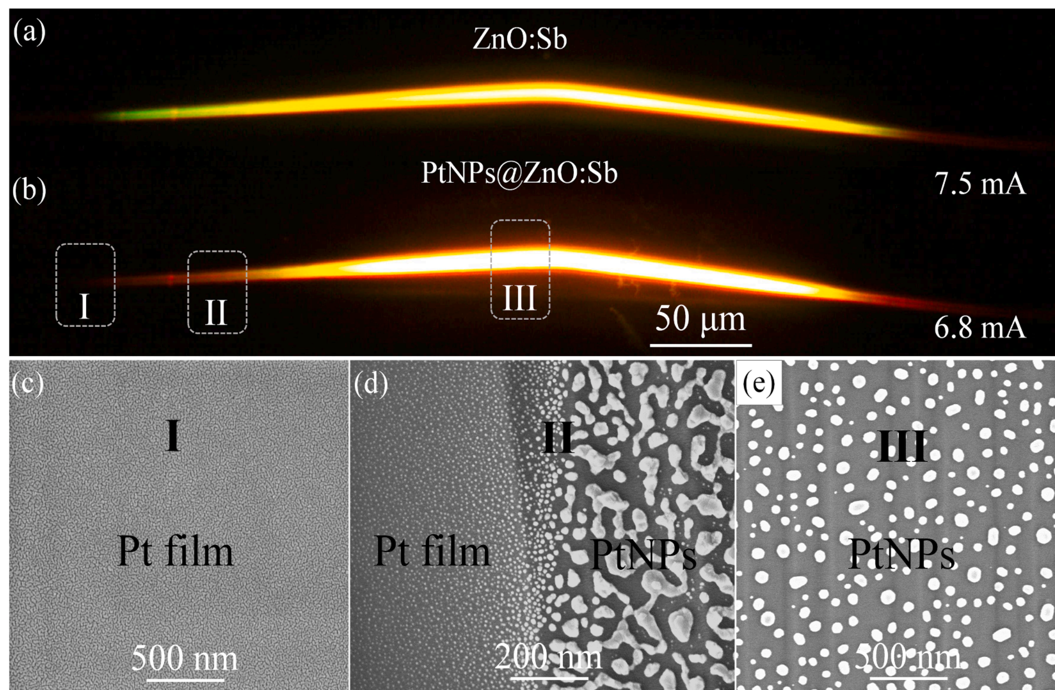

Fig. 3. The morphological characterizations of a single ZnO:Sb MW undecorated and decorated by Pt nanostructures. (a) Optical microscope EL image of a single ZnO:Sb MW based fluorescent filament light source, the light source was operated at a driving current of 7.5 mA. (b) Optical microscope EL image of a fluorescent filament light source, in which the ZnO:Sb MW was covered by Pt nanofilm (the injection current ∼ 6.8 mA). (c) SEM image of Pt nanofilms, which has been deposited on ZnO:Sb MW (∼**I**). (d) SEM graph of the marked **II** in (b), which corresponds to the critical area between the lighting and non-lighting. In **II**-region, the evolution of Pt changing from quasiparticle film to isolated and hemispherical nanoparticles can be achieved. (e) SEM image of physically isolated PtNPs, which has been prepared on the ZnO:Sb wire (∼**III**).

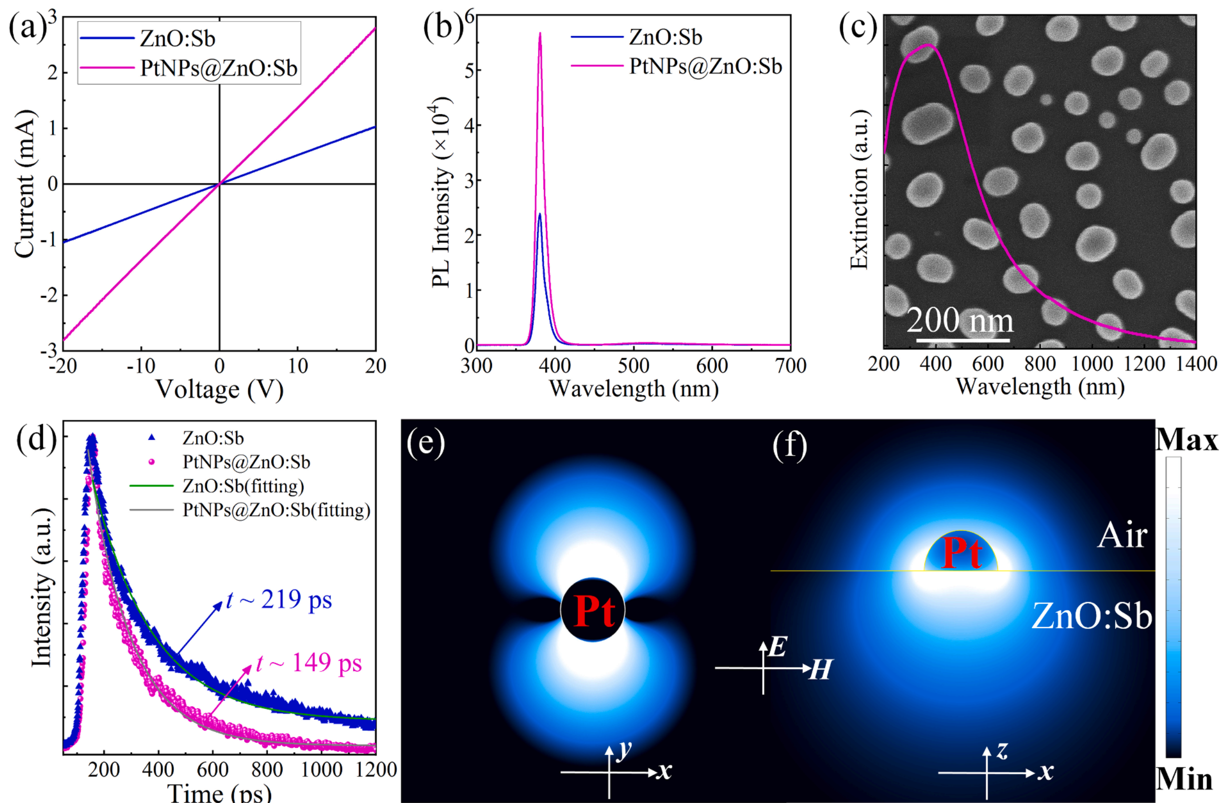

Fig. 4. Characterizing the modulation of PtNPs on the electrical and optical features of an individual ZnO:Sb MW. (a) I-V curves of a single ZnO:Sb MW, and the wire coated by PtNPs. (b) PL spectra of a single ZnO:Sb MW, and the sample coated by PtNPs. (c) Normalized extinction spectrum of as-synthesized PtNPs. Inset: SEM figure of PtNPs sample. (d) TRPL results of a pristine ZnO:Sb MW, and the wire decorated by PtNPs. (e) Theoretically simulated electric-field intensities of an isolated PtNP, which placed on ZnO:Sb (*x*-*y* plane). (f) The calculated electric-field intensities at the PtNP/ZnO:Sb interface, which is corresponding to *x*-*z* plane.

The influence of PtNPs on the optical and electrical features of ZnO:Sb wires were studied. Fig. 4(a) illustrates I-V curves of an individual ZnO:Sb MW without and with PtNPs cladding. Apart from the enhancement of electronic transport properties, the linear feature indicates that the formation of ohmic contacting between ZnO:Sb MW and Ag pastes electrodes. Previous literature reported that surface morphologies of low-dimensional ZnO play a crucial role on current transport across the Au-ZnO interface. The underlying factors, which involving the surface states, crystallization quality, charge carrier' depletion layer and band bending caused by surface influences, have a distinct modulation on ZnO:Sb barrier heights [18,39]. The modulation could be principally assigned to Fermi level pinning or metal-induced gap states when contacting with the nearby semiconductor. Due to the relatively higher crystallization quality of CVD-synthesized ZnO:Sb samples, the Schottky barrier created at Pt/ZnO:Sb interface makes little effect on the current transport characteristics of an individual ZnO:Sb MW. Consequently, the observably enhanced electronic transport behavior observed in a ZnO:Sb MW can be assigned to the surface treatment by capping PtNPs [51,53,55].

Upon optical excitation by a He-Cd laser, PL properties of an individual ZnO:Sb MW not decorated and decorated by PtNPs were checked. The PL spectra are depicted in Fig. 4(b). Shown in the figure, the PtNPs coating (the diameter $d \sim 80$ nm) can be used to enhance intensity of ultraviolet emission in contrast to that of the pristine MW. While, there is little variation of the visible emission in the single ZnO:Sb MW uncovered and covered by PtNPs. In addition to the protective capping and surface passivation, the enhancement in PL intensity based on an individual ZnO:Sb MW is ascribed to the cooperative effect of surface reconstructing and positive suppression of non-radiative recombination centers with the aid of PtNPs decoration. Further to precisely exhibit the influence of PtNPs with appropriate sizes on the photoelectrical properties of an individual ZnO:Sb MW, the ultraviolet plasmonic response was researched. The synthesis of PtNPs with identical size was implemented, as we mentioned in the Experimental Section. The sample of PtNPs that has been synthesized on the quartz substrate was shown in the inset of Fig. 4(b). Clearly, the sizes of these nanoparticles were averagely identical to those being prepared on the ZnO:Sb wire. Optical characteristics of these PtNPs were studied using ultraviolet–visible extinction spectroscopy. Fig. 4(c) exhibits their extinction spectrum, in which the dominant peak was found at 365 nm. Thereby, the achieved emission enhancement in the PtNPs@ZnO:Sb MWs can be assigned to coupling between PtNPs plasmons and ZnO:Sb excitons [28,51,56]. To gain deeply understanding the coupling mechanism, time-resolved PL (TRPL) tests of a single ZnO:Sb MW uncovered and covered by PtNPs were carried out at room temperature, and the TRPL curves are shown in Fig. 4(d). The decay lifetime τ is described as the formula

$$I(t) = I_0 exp(-t/\tau) \tag{2}$$

In this formula, I_0 is a constant [56]. Illustration in the figure, the decay lifetime of the PtNPs@ZnO:Sb MW was evaluated to approximately 149 ps, which is dramatically smaller than that of the pristine sample (~219 ps). The spontaneous emission decay rate of ZnO:Sb MW is dramatically increased owing to Purcell effect. The result illustrates that the PtNPs coating can facilitate the electron-holes recombination in the ZnO:Sb MW, providing the plasmon-mediated resonance coupling between the ZnO:Sb excitons and PtNPs plasmons [28,51,54].

Further, theoretical analysis and simulation was promised to study the coupling between PtNPs and ZnO:Sb MW. In the simulation, a linearly polarized plane wave was illuminated on the target. In the simulation regime, a perfect structured PtNP immersed on the ZnO:Sb MW was built. The use of PtNPs was modeled as a hemispherical cap. The wavelength of incident plane wave is 365 nm, $n_{ZnO:Sb}$ is about 2.35.

Fig. 4(e) displays the simulated electric-field distribution around a single Pt nanostructure, which is placed on the ZnO:Sb (*x-y* plane). The result exhibits that the strongest distribution of the simulated electric-field is primarily centralized at two sides of the PtNP as the wavelength of illuminated light was matched well with the dominant extinction peak of PtNPs. Fig. 4(f) represents the distribution of simulated electric-field at PtNP/ZnO:Sb interface, which corresponds to the cross section at *x-z* plane. Illustration in the figure, the calculated electric-field intensity is principally localized at the PtNPs/ZnO:Sb interface. And the localized electric-field intensities were due to the excitation of localized surface plasmon resonances of PtNPs. Besides, the calculated electric-field can also permeate into neighboring ZnO:Sb MW, accompanying by a sharp decaying with an increase of the gap distance from the PtNPs to the neighboring ZnO:Sb. That is, PtNPs can plasmonically reorganize the electric-field distribution. Therefore, when excited plasmonically, the PtNPs can concentrate the optical energy intensively at the PtNPs/ZnO:Sb interface, facilitating the radiation recombination rate of electron-hole pairs [28,49,56].

As described above, an individual ZnO:Sb MW uncovered and covered by PtNPs were developed to fabricate homojunction LEDs, in which *n*-type ZnO film was employed as electron transporting source [11,26,36]. Schematic image of the fabricated p-PtNPs@ZnO:Sb MW/*n*-ZnO homojunction LED is depicted in Fig. 5(a). Electrical properties of the fabricated homojunction devices were performed, and the corresponding current–voltage (I-V) characteristics are plotted in Fig. 5(b). Shown in the figure, I-V curve of the pristine p-ZnO:Sb MW/*n*-ZnO homostructure device exhibits a nice rectifying characteristics, and the $I_{+20\ V}/I_{-20\ V}$ is extracted to about 8. The threshold voltage was estimated to about 3.22 V. The result implies that a high-quality p-n homojunction is achieved due to the good Ohmic contacting properties between Au electrodes and ZnO:Sb MW/ZnO substrate [35,36]. While introducing PtNPs decoration, I-V curve (the violet solid line) reveals that the rectification value of the fabricated p-PtNPs@ZnO:Sb MW/*n*-ZnO homojunction LED can reach up to 20, which is observable higher than that of the pristine homojunction. By a comparison, the incorporation of PtNPs coating can result in significant increase of electrical properties of the as-constructed p-PtNPs@ZnO:Sb MW/*n*-ZnO homojunction. Apart from the LED-like rectification features, the threshold voltage of the PtNPs@ZnO:Sb MW homojunction device is distinctly reduced to about 2.55 V. Although, much larger leakage current could be observed in the reverse voltage. The clearly enhanced electronic transport properties in the fabricated p-PtNPs@ZnO:Sb MW/*n*-ZnO homojunction LED is attributed to the significant decrease of the contacting resistance by cladding PtNPs, thus achieving the efficient transport and injection of charge carriers in the ZnO:Sb MW active media in the as-constructed LEDs [26,51].

Under external bias above the turn-on voltage, EL emission can occur toward the p-n junction interface and the emitted photons can escape from the sharp edges from ZnO:Sb MW. The emitted photons were recorded by a microscope objective. The EL spectra of the fabricated homojunction structured LEDs under different forward bias were measured using a spectrometer. Fig. 5(c) presents the EL spectra of our constructed p-ZnO:Sb MW/*n*-ZnO homojunction LED. It is obviously seen that, a strong and broad ultraviolet emission band appeared at around 378.5 nm under various currents varying from 0.8 to 7.6 mA. Significantly, the defect-related luminescence in the visible wavelengths, which have been currently obtained in previously reported ZnO hetero/homojunction light sources, is absent [38,43,44,52]. The EL

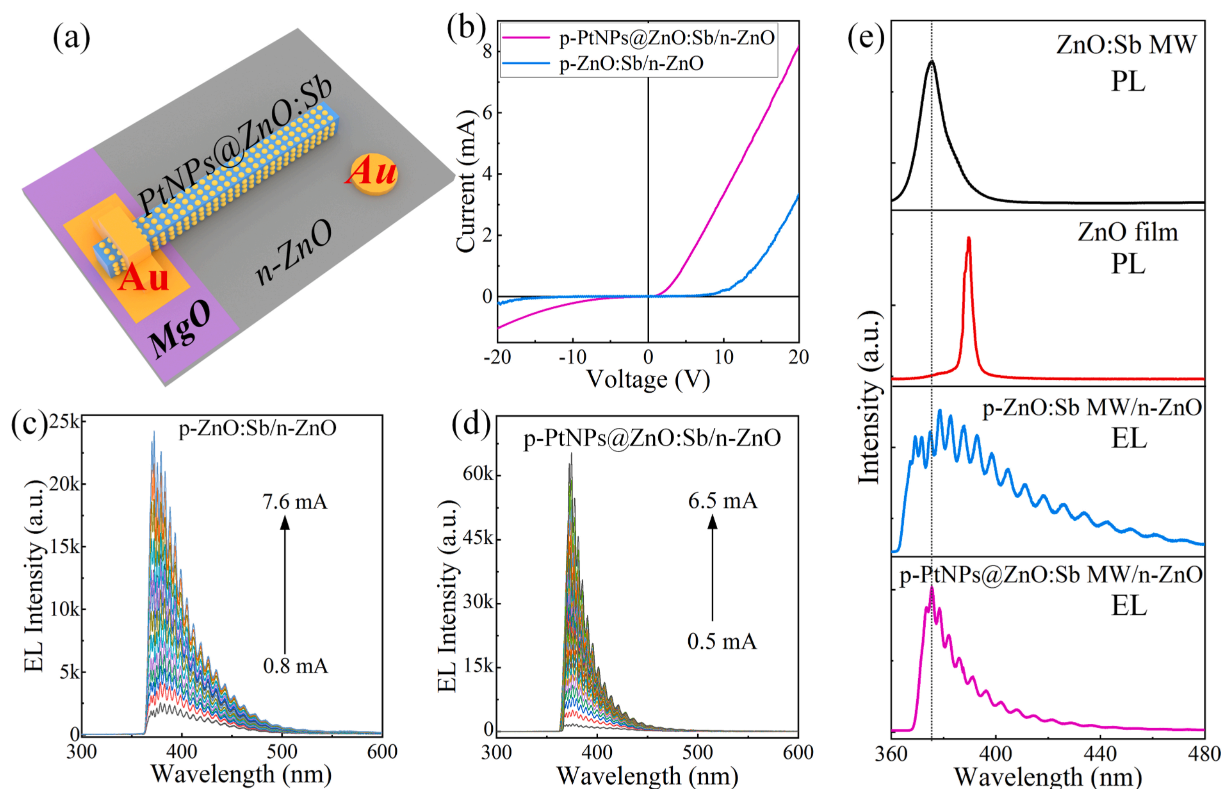

Fig. 5. Comparison of the as-constructed single MW homojunction LEDs, in which an individual ZnO:Sb MW was undecorated and decorated by PtNPs with appropriate sizes. (a) Three-dimensional model describing the detailed structure of as-designed single wire homojunction LED, containing a p-type ZnO:Sb MW covered by PtNPs and *n*-type ZnO layer. Au nanfilms contact were employed as the electrodes for the current injection. (b) The I-V characteristics curves of our homojunction LED light sources. In the LED structure, ZnO:Sb MW was undecorated and decorated by PtNPs. (c) EL spectra of electrically-biased p-ZnO:Sb MW/*n*-ZnO homojunction LED. The operating current varied ranging from 0.8 to 7.6 mA. (d) EL spectra of electrically biased p-PtNPs@ZnO:Sb MW/*n*-ZnO homojunction LED, with the injection varying from 0.5 to 6.5 mA. (e) Normalized PL spectra of ZnO:Sb MW and ZnO film, and normalized EL intensities of our constructed LEDs are given for a comparison (The driving current is fixed at a current of 5.2 mA).

Optics and Laser Technology 160 (2023) 109052

peak positions are nearly consistent with the PL measurements, which have been shown in Fig. 4(b). Thus, it is visibly evidenced that the broad ultraviolet EL is mainly originated from the ZnO:Sb wire. No significant shift in the EL peak positions could be observed even operated at high driving current level. The resulting ultraviolet EL emissions are primarily related to the fabricated p-ZnO:Sb/*n*-ZnO homojunction. Thus, the quantum-confined Stark effect is absent [8,11,53]. Besides, with an increase of the operating current, the dependence of EL intensity on the operating current exhibits a linear manner. The approximatively linear behavior suggested our fabricated an individual ZnO:Sb MW based light source has a competent p-n junction characteristics, and can achieve sufficiently-high recombination efficiency when operated as the driving current at high levels. Similarly, when biased electrically, EL characterization of our constructed p-PtNPs@ZnO:Sb MW/*n*-ZnO homojunction LED was carried out. Fig. 5(d) illustrates its EL spectra, revealing a strong ultraviolet ELs positioning at around 375.0 nm. Especially, the line width was averagely extracted to about 20 nm, which is significantly narrower than that of the pristine homojunction LED. In a consequence, the introduction of PtNPs can be used to purify the EL behaviors of our fabricated p-ZnO:Sb MW/*n*-ZnO homojunction LEDs [8,11,53]. Detailed information on the EL characteristics will be discussed below.

To deeply understand the EL mechanism of the fabricated homojunction LEDs, normalized EL intensities of fabricated single MW homojunction LEDs operated at a forward injection current ~ 5.25 mA are plotted in Fig. 5(e). Besides, normalized PL intensities of ZnO:Sb MW and ZnO film were also compared, as shown in Fig. 5(e). The dominant wavelength of ZnO:Sb MW PL is centered at around 375.2 nm with the linewidth of about 12.5 nm, while the main peak of ZnO film PL emission was positioned at around 389.7 nm and linewidth of about 5.0 nm. By contrast, the dominant EL wavelengths of our fabricated homojunction LEDs without and with PtNPs cladding were primarily centered in the ultraviolet regions. Although all the ultraviolet EL emissions of our fabricated homojunction LEDs are dominated by the band-edge luminescence of ZnO:Sb MW, the profiles of the EL spectra represent great differences. The line width of the p-PtNPs@ZnO:Sb MW/*n*-ZnO homojunction LED is derived to about 20 nm, which is much narrower than that of the pristine homojunction device (~40 nm). In this case, the EL of our constructed p-ZnO:Sb MW/*n*-ZnO homojunction LED can emerge from the ZnO:Sb MW, p-ZnO:Sb/*n*-ZnO interface and ZnO film, respectively [36,52]. Because of the higher carrier concentration and mobility in *n*-type ZnO film, the transport of injected electron from ZnO film could win over the hole injection, which is originated from the p-type ZnO:Sb MW. In a consequence, the EL emission is determined primarily by electron injection from the ZnO film to the ZnO:Sb MW in the as-constructed p-ZnO:Sb MW/*n*-ZnO homojunction LED. The radiative recombination is mainly distributed in the ZnO:Sb MW [8,11,26]. Additionally, the fine structure of EL spectra with multimode subpeaks illustrates a group of resonance fringes, which is associated with typical FP microresonator in the quadrilateral ZnO:Sb MW. Q-factor of the supreme multipeak is evaluated to about 210 of the p-PtNPs@ZnO:Sb MW/*n*-ZnO homojunction LED, which is visibly higher than that of the pristine homojunction emission device (Q-factor ~ 180). Benefited from the covered PtNPs, the radiative recombination in p-ZnO:Sb MW/*n*-ZnO homojunction LED can be successfully modulated, and then finally concentrated in the ZnO:Sb MW gain medium [26,55]. Consequently,

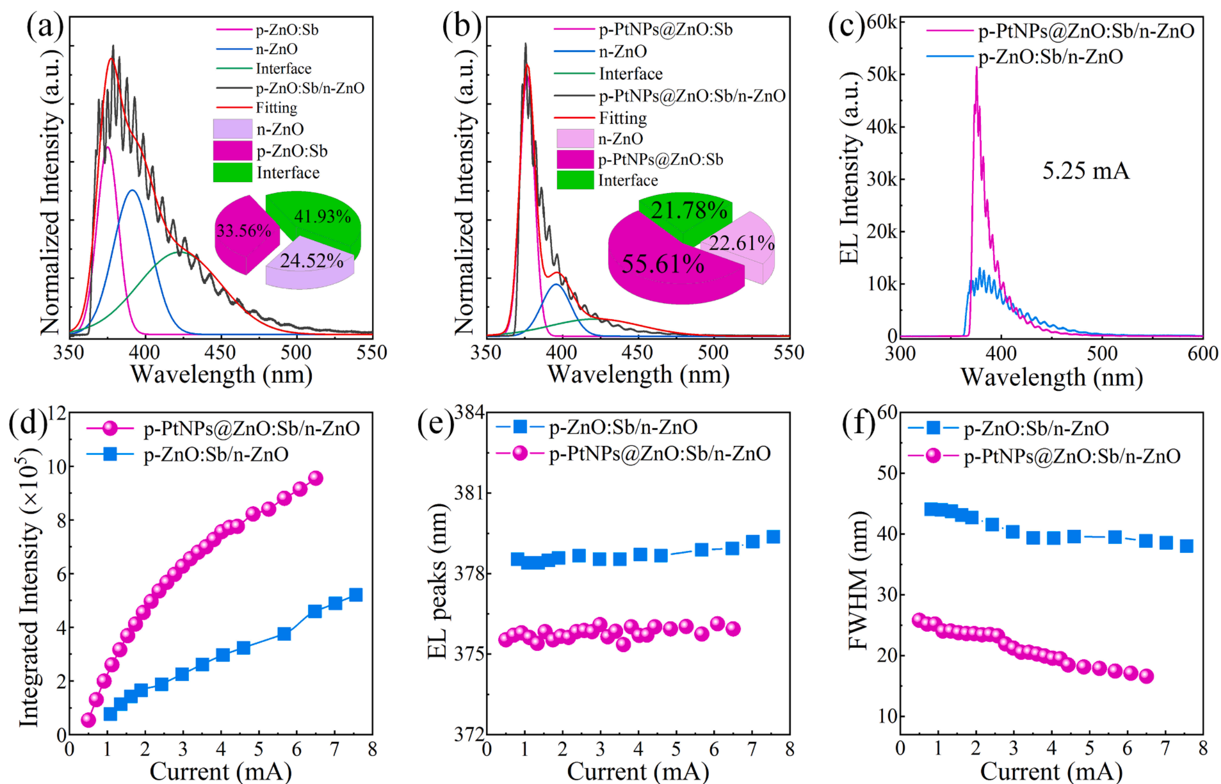

Fig. 6. The effect of PtNPs on the EL properties of the pristine p-ZnO:Sb MW/*n*-ZnO homojunction LED. (a) EL spectrum of the pristine p-ZnO:Sb MW/*n*-ZnO homojunction LED via Gaussian fitting (the forward current ~ 5.25 mA). Inset: The content of ZnO film emission, ZnO:Sb MW emission and p-ZnO:Sb/*n*-ZnO interfacial emission. (b) EL spectrum of as-constructed p-PtNPs@ZnO:Sb MW/*n*-ZnO homojunction LED via Gaussian fitting (the forward current ~ 5.25 mA). Inset: The content of ZnO film emission, PtNPs@ZnO:Sb MW emission and p-PtNPs@ZnO:Sb/*n*-ZnO interfacial emission. (c) EL spectra of our designed ZnO:Sb MW homojunction LEDs without and with PtNPs coating were given for a comparison when plotted at an operating current of 5.25 mA. (d) The dependence of integrated EL intensity of as-constructed single ZnO:Sb MW homojunction LEDs without and with PtNPs decoration in terms of injection current. (e) The variations of the main EL peaks of our prepared homojunction LEDs versus the injection current. (f) The variations of the FWHM of as-prepared homojunction LEDs versus the injection current.

the ultraviolet EL emission, which was derived from the as-synthesized ZnO:Sb MW active region, can be dramatically increased with the aid of plasmonic response of the deposited PtNPs [28,50,56].

To probe into the effect of PtNPs on the EL behaviors of our fabricated ZnO:Sb MW homojunction LEDs, Gaussian fitting was applied to analyze the emission spectra, which were recorded at a driving current of 5.25 mA. The fitted EL spectrum via subpeak deconvolution for the pristine p-ZnO:Sb MW/*n*-ZnO homojunction LED is shown in Fig. 6(a). Illustrated in the image, the EL spectrum is comprised of three distinct bands peaking at around 374.5 nm, 391.5 nm, and 418.0 nm, respectively. Compared with the emission spectra in Fig. 5(e), the wavelengths of the luminescence center for broadband ultraviolet emission at 374.5 and 391.5 nm are originated from typical band-edge recombination in the CVD-synthesized ZnO:Sb sample and ZnO layer, respectively. While the light-emission peaking at 418.0 nm could be resulted from the interfacial recombination of the electrons in *n*-ZnO layer and holes in p-type ZnO:Sb MW. The content of ultraviolet emission, especially for the light-emitting occurring in the ZnO:Sb MW in the pristine homojunction LED, was calculated to about 33.56 %. By covering PtNPs on the ZnO:Sb MW, the typical EL spectrum of our p-PtNPs@ZnO:Sb MW/*n*-ZnO homojunction LED can be decomposed into three different Gaussian parts, as displayed in Fig. 6(b). Illustration in the image, the obtained EL emission of the as-constructed LED was primarily dominated by the near-band-edge recombination occurring in the ZnO:Sb MW channel. And the light-emission content of ZnO:Sb MW in the treated LEDs was estimated to about 55.61 %. This value is explicitly larger than that of the pristine homojunction LED. Therefore, cladding PtNPs with appropriate plasmonic response can be used to purify the ultraviolet emissions of our proposed p-ZnO:Sb MW/*n*-ZnO homojunction LEDs.

When recorded at a forward driving current of 5.25 mA, EL spectra of the constructed homojunction LEDs without and without PtNPs cladding were shown in Fig. 6(c) to make a comparison. Illustration in the image, a 4.5-fold enhancement of the EL peak intensity was achieved. Fig. 6(d) demonstrates the curves of integrated EL intensities versus the forward driving current for the fabricated an individual MW homojunction LED light sources, respectively. The integrated EL intensities of the p-PtNPs@ZnO:Sb MW/*n*-ZnO homojunction LED are significantly larger than that of the pristine device at each input current. The result suggests that the incorporation of PtNPs coating can effectively enhance the EL efficiency of p-ZnO:Sb MW/*n*-ZnO homojunction LED. The influence of PtNPs on EL properties of our fabricated homojunction LEDs was researched in more detail. Fig. 6(e) depicts the dependence of the dominant EL wavelengths on the forward operating currents. A slight shift of the EL peaks toward longer wavelengths of the fabricated homojunction LEDs can be observed, which could be derived from the junction heating at high injection levels. Taken the p-ZnO:Sb MW/*n*-ZnO homojunction LED for example, the junction heating can yield an approximate 1.0 nm red shift of the predominant ultraviolet peak at 378.5 nm as the current increasing in the range of 0.8–7.6 mA; while the junction heating could only result in a 0.5 nm red shift the dominated ultraviolet peak at 375.5 nm. As the integrated EL intensities of our constructed LEDs increase linearly, the radiative recombination rate that primarily centralized in the ZnO:Sb MWs is not influenced by the high junction temperature, which underlining that the CVD-synthesized ZnO:Sb samples are the most likely the significant constituents for constructing droop-free LEDs and microlaser devices [8,11,26].

The dependence of EL linewidth of the fabricated homojunction LEDs on the operating current is represented in Fig. 6(f). Shown in the image, the EL linewidth of the pristine p-ZnO:Sb MW/*n*-ZnO homojunction LED was averagely extracted to about 40 nm, accompanying by a visible narrowing tendency in the range of 45–40 nm. Introducing PtNPs with desired plasmons, the EL profiles exhibit an observable narrower linewidth ~ 20 nm on average. By a comparison, the recombination regions that appearing in the ZnO film and occurring at the p-ZnO:Sb/*n*-ZnO homointerface could be suppressed availably. Especially for the p-PtNPs@ZnO:Sb MW/*n*-ZnO homojunction LED, the reduction in the EL linewidth varying from 31.5 to 16.6 nm can be obtained with an increase of the operating current, implying a gradual suppression of electron-hole recombination in the ZnO film and toward the p-ZnO:Sb/*n*-ZnO interface. The obtained narrower EL linewidth at high injection regime is comparable to the PL of CVD-grown ZnO:Sb MW in this wavelength range. Consequently, Auger recombination and electron overflow induced EL droop in the pristine ZnO:Sb MW homojunction can be suppressed [8]. Introducing a layer of PtNPs decoration, the predominant emission features of the obtained EL spectra for the LEDs were consistently in agreement with those of the PL results obtained for the CVD-synthesized ZnO:Sb samples, thus realizing typical electron-hole recombination in the PtNPs@ZnO:Sb MW active region. These unique homojunction ultraviolet LEDs exhibit highly stable emission and negligible efficiency droop [11,26,45].

4. Conclusions

In summary, we have designed and prepared a facile and low-cost project to construct low-dimensional ZnO homojuntion ultraviolet LED, which is constituted by a ZnO:Sb MW covered by PtNPs as the p-type component, and *n*-type ZnO film serving as *n*-type component. The fabricated single MW homojunction LED can emit at an EL wavelength of 375.5 nm and a linewidth of about 16.6 nm at high operating current levels, thus achieving high-efficiency excitonic radiative recombination in the ZnO:Sb MW gain region. In the LED structure, the usage of individual ZnO:Sb MW can act as the active region of the homojunction LED and generate a narrow-band ultraviolet emission with the aid of plasmonic PtNPs. Thus, the preparation of genuine p-type ZnO low-dimensional structures with good stability, reliability and repeatability is imperative to fabricate highly efficient ZnO homojunction LEDs and LDs featuring in the ultraviolet wavelengths. The experimental results express a revolutionary progress aiming at the application of low-dimensional p-type ZnO in developing luminescence/lasing devices, and provides an important research strategy toward future fabrication technique for ZnO homojunction optoelectronic devices.

CRediT authorship contribution statement

Dailong Wang: Conceptualization, Methodology, Writing – original draft. **Maosheng Liu:** Methodology, Formal analysis, Data curation, Conceptualization. **Shenao Shang:** . **Peng Wan:** Formal analysis. **Daning Shi:** Supervision, Funding acquisition. **Caixia Kan:** Conceptualization, Funding acquisition, Supervision. **Binghui Li:** Conceptualization. **Mingming Jiang:** Conceptualization, Supervision, Resources, Methodology, Data curation, Funding acquisition, Writing – review & editing.

Declaration of Competing Interest

The authors declare that they have no known competing financial interests or personal relationships that could have appeared to influence the work reported in this paper.

Data availability

Data will be made available on request.

Acknowledgements

This study was supported by the National Natural Science Foundation of China (Grant Nos. 11974182, 11874220), the Fundamental Research Funds for the Central Universities (NO. NC2022008), and Funding for Outstanding Doctoral Dissertation in NUAA (BCXJ22-14).

References

[1] J. Chen, S. Loeb, J.-H. Kim, LED revolution: fundamentals and prospects for UV disinfection applications, Environ. Sci.: Water Res Technol. 3 (2017) 188–202.
[2] W.-K. Jo, R.J. Tayade, New generation energy-efficient light source for photocatalysis: LEDs for environmental applications, Ind. Eng. Chem. Res. 53 (6) (2014) 2073–2084.
[3] T.-R. Kwon, S.-E. Lee, J.H. Kim, Y.N. Jang, S.-Y. Kim, S.K. Mun, C.W. Kim, J. Na, B. J. Kim, 310 nm UV-LEDs attenuate imiquimod induced psoriasis-like skin lesions in C57BL/6 mice and inhibit IL-22-induced STAT3 expression in HaCaT cells, Photochem. Photobiol. Sci. 19 (8) (2020) 1009–1021.
[4] X. Fang, Y. Bando, U.K. Gautam, T. Zhai, H. Zeng, X. Xu, M. Liao, D. Golberg, ZnO and ZnS nanostructures: Ultraviolet-light emitters, lasers, and sensors, Crit. Rev. Solid State 34 (3–4) (2009) 190–223.
[5] J. Liu, H. Chen, L. Ma, Z. He, D. Wang, Y. Liu, Q. Lin, T. Zhang, N. Gray, H. U. Kaniskan, J. Jin, W. Wei, Light-induced control of protein destruction by opto-PROTAC, Sci. Adv. 6 (8) (2020) eaay5154.
[6] J. Shi, M. Li, H. Tang, J. Kang, N. Sharmin, A. Rosenthal, K.K.Y. Wong, Hybrid optical parametrically-oscillating emitter at 1930 nm for volumetric photoacoustic imaging of water content, eLight 2 (2022) 6.
[7] Y. Li, P.N. Nesterenko, B. Paull, R. Stanley, M. Macka, Performance of a new 235 nm UV-LED-based on-capillary photometric detector, Anal. Chem. 88 (24) (2016) 12116–12121.
[8] B. Nikoobakht, R.P. Hansen, Y. Zong, A. Agrawal, M. Shur, J. Tersoff, High-brightness lasing at submicrometer enabled by droop-free fin light-emitting diodes (LEDs), Sci. Adv. 6 (33) (2020) eaba4346.
[9] X.-S. Fang, C.-H. Ye, L.-D. Zhang, Y. Li, Z.-D. Xiao, Formation and optical properties of thin and wide tin-doped ZnO nanobelts, Chem. Lett. 34 (3) (2005) 436–437.
[10] J. Li, N. Gao, D. Cai, W. Lin, K. Huang, S. Li, J. Kang, Multiple fields manipulation on nitride material structures in ultraviolet light-emitting diodes, Light: Sci Appl. 10 (2021) 129.
[11] S. Chu, G. Wang, W. Zhou, Y. Lin, L. Chernyak, J. Zhao, J. Kong, L. Li, J. Ren, J. Liu, Electrically pumped waveguide lasing from ZnO nanowires, Nature Nanotech. 6 (8) (2011) 506–510.
[12] H. Chang, Z. Liu, S. Yang, Y. Gao, J. Shan, B. Liu, J. Sun, Z. Chen, J. Yan, Z. Liu, J. Wang, P. Gao, J. Li, Z. Liu, T. Wei, Graphene-driving strain engineering to enable strain-free epitaxy of AlN film for deep ultraviolet light-emitting diode, Light: Sci Appl. 11 (2022) 88.
[13] Y.i. Sun, K. Zhou, M. Feng, Z. Li, Y.u. Zhou, Q. Sun, J. Liu, L. Zhang, D. Li, X. Sun, D. Li, S. Zhang, M. Ikeda, H. Yang, Room-temperature continuous-wave electrically pumped InGaN/GaN quantum well blue laser diode directly grown on Si, Light Sci Appl 7 (1) (2018).
[14] M.N. Sharif, M. Ajmal Khan, Q. Wali, I. Demir, F. Wang, Y. Liu, Performance enhancement of AlGaN deep-ultraviolet laser diode using compositional Al-grading of Si-doped layers, Opt. Laser Technol. 152 (2022), 108156.
[15] K.H. Li, X. Liu, Q. Wang, S. Zhao, Z. Mi, Ultralow-threshold electrically injected AlGaN nanowire ultraviolet lasers on Si operating at low temperature, Nature Nanotech 10 (2) (2015) 140–144.
[16] J. Stachurski, S. Tamariz, G. Callsen, R. Butte, N. Grandjean, Single photon emission and recombination dynamics in self-assembled GaN/AlN quantum dots, Light: Sci Appl. 11 (2022) 114.
[17] J. Wang, M. Wang, F. Xu, B. Liu, J. Lang, N. Zhang, X. Kang, Z. Qin, X. Yang, X. Wang, W. Ge, B. Shen, Sub-nanometer ultrathin epitaxy of AlGaN and its application in efficient doping, Light: Sci Appl. 11 (2022) 71.
[18] Z. Ma, G. Li, X. Zhang, J. Li, C. Zhang, Y. Ma, J. Zhang, B. Leng, N. Usoltseva, V. An, B. Liu, High-performance and broadband photodetection of bicrystalline $(GaN)_{1-x}(ZnO)_x$ solid solution nanowires via crystal defect engineering, J. Mater. Sci. Technol. 85 (2021) 255–262.
[19] Z. Zheng, Q. Chen, J. Dai, A. Wang, R. Liang, Y. Zhang, M. Shan, F. Wu, W. Zhang, C. Chen, X. Li, Enhanced light extraction efficiency via double nano-pattern arrays for high-efficiency deep UV LEDs, Opt. Laser Technol. 143 (2021), 107360.
[20] I.M. Hoiaas, A. Liudi Mulyo, P.E. Vullum, D.-C. Kim, L. Ahtapodov, B.-O. Fimland, K. Kishino, H. Weman, GaN/AlGaN nanocolumn ultraviolet light-emitting diode using double-layer graphene as substrate and transparent electrode, Nano Lett. 19 (3) (2019) 1649–1658.
[21] W.-B. Jung, S. Jang, S.-Y. Cho, H.-J. Jeon, H.-T. Jung, Recent progress in simple and cost-effective top-down lithography for $\approx$ 10 nm scale nanopatterns: from edge lithography to secondary sputtering lithography, Adv. Mater. 32 (35) (2020) 1907101.
[22] R.C. Subedi, J.-W. Min, S. Mitra, K.-H. Li, I. Ajia, E. Stegenburgs, D.H. Anjum, M. Conroy, K. Moore, U. Bangert, I.S. Roqan, T.K. Ng, B.S. Ooi, Quantifying the transverse-electric-dominant 260 nm emission from molecular beam epitaxy-grown GaN-quantum-disks embedded in AlN nanowires: a comprehensive optical and morphological characterization, ACS Appl. Mater. Interfaces 12 (37) (2020) 41649–41658.
[23] G. Zhu, J. Li, J. Li, J. Guo, J. Dai, C. Xu, Y. Wang, Single-mode ultraviolet whispering gallery mode lasing from a floating GaN microdisk, Opt. Lett. 43 (4) (2018) 647–650.
[24] H.e. Shen, C.-X. Shan, Q. Qiao, J.-S. Liu, B.-H. Li, D.-Z. Shen, Stable surface plasmon enhanced ZnO homojunction light-emitting devices, J. Mater. Chem. C 1 (2) (2013) 234–237.
[25] W. Ouyang, J. Chen, Z. Shi, X. Fang, Self-powered UV photodetectors based on ZnO nanomaterials, Appl. Phys. Rev. 8 (3) (2021) 031315.
[26] X. Zhou, M. Jiang, K. Xu, M. Liu, S. Sha, S. Cao, C. Kan, D.N. Shi, Electrically driven single microwire-based single-mode microlaser, Light: Sci Appl. 11 (2022) 198.
[27] P. Wan, M. Jiang, T. Xu, Y. Liu, C. Kan, High-mobility induced high-performance Self-powered ultraviolet photodetector based on single ZnO microwire/PEDOT:PSS heterojunction via slight Ga-doping, J. Mater. Sci. Technol. 93 (2021) 33–40.
[28] M. Liu, M. Jiang, X. Zhou, C. Kan, D. Shi, Performance-enhanced single-mode microlasers in an individual microwire covered by Ag nanowires, Opt. Laser Technol. 155 (2022), 108391.
[29] C. Xu, J. Dai, G. Zhu, G. Zhu, Y. Lin, J. Li, Z. Shi, Whispering-gallery mode lasing in ZnO microcavities, Laser Photonics Rev. 8 (4) (2014) 469–494.
[30] Y. Chen, L. Su, M. Jiang, X. Fang, Switch type PANI/ZnO core-shell microwire heterojunction for UV photodetection, J. Mater. Sci. Technol. 105 (2022) 259–265.
[31] Z. Li, M. Jiang, Y. Sun, Z. Zhang, B. Li, H. Zhao, C. Shan, D. Shen, Electrically pumped Fabry-Perot microlasers from single Ga-doped ZnO microbelt based heterostructure diodes, Nanoscale 10 (39) (2018) 18774–18785.
[32] Q. Bao, W. Li, P. Xu, M. Zhang, D. Dai, P. Wang, X. Guo, L. Tong, On-chip single-mode CdS nanowire laser, Light: Sci Appl. 9 (1) (2020) 42.
[33] H. Dang, X. Zhou, B. Li, C. Kan, M. Jiang, Higher-performance Fabry-Perot microlaser enabled by a quadrilateral microwire via Ag nanowires decoration, Opt. Mater. 120 (2021), 111419.
[34] Y. Wu, Y. Ren, A. Chen, Z. Chen, Y. Liang, J. Li, G. Lou, H. Zhu, X. Gui, S. Wang, Z. Tang, A one-dimensional random laser based on artificial high-index contrast scatterers, Nanoscale 9 (21) (2017) 6959–6964.
[35] P. Wan, M. Jiang, T. Xu, Y. Liu, X. Fang, C. Kan, Doping concentration influenced pyro-phototronic effect in self-powered photodetector based on Ga-incorporated ZnO microwire/p^+-GaN heterojunction, Adv. Opt. Mater. 10 (2) (2022) 2101851.
[36] G. He, M. Jiang, B. Li, Z. Zhang, H. Zhao, C. Shan, D. Shen, Sb-Doped ZnO microwires: emitting filament and homojunction light-emitting diodes, J. Mater. Chem. C 5 (2017) 10938–10946.
[37] W. Liu, F. Xiu, K. Sun, Y.-H. Xie, K.L. Wang, Y. Wang, J. Zou, Z. Yang, J. Liu, Na-doped p-Type ZnO microwires, J. Am. Chem. Soc. 132 (8) (2010) 2498–2499.
[38] A. Chen, H. Zhu, Y. Wu, M. Chen, Y. Zhu, X. Gui, Z. Tang, Beryllium-assisted p-Type doping for ZnO homojunction light-emitting devices, Adv. Funct. Mater. 26 (21) (2016) 3696–3702.
[39] Z. Huo, X. Wang, Y. Zhang, B. Wan, W. Wu, J. Xi, Z. Yang, G. Hu, X. Li, C. Pan, High-performance Sb-doped p-ZnO NW films for self-powered piezoelectric strain sensors, Nano Energy 73 (2020), 104744.
[40] S. Limpijumnong, S.B. Zhang, S.-H. Wei, C.H. Park, Doping by large-size-mismatched impurities: The microscopic origin of arsenicor antimony-doped *p*-type zinc oxide, Phys. Rev. Lett. 92 (2004), 155504.
[41] Y.-J. Lu, H.-F. Li, C.-X. Shan, B.-H. Li, D.-Z. Shen, L.-G. Zhang, S.-F. Yu, Improved performance of ZnO light-emitting devices by introducing a hole-injection layer, Opt. Express 22 (14) (2014) 17524–17531.
[42] S.-D. Baek, P. Biswas, J.-W. Kim, Y.C. Kim, T.I. Lee, J.-M. Myoung, Low-temperature facile synthesis of Sb-doped p-Type ZnO nanodisks and its application in homojunction light-emitting diode, ACS Appl. Mater. Interfaces 8 (20) (2016) 13018–13026.
[43] M. Su, T. Zhang, J. Su, Z. Wang, Y. Hu, Y. Gao, H. Gu, X. Zhang, Homogeneous ZnO nanowire arrays p-n junction for blue light-emitting diode applications, Opt. Express 27 (16) (2019) A1207–A1215.
[44] Q.-J. Feng, H.-W. Liang, Y.-Y. Mei, J.-Y. Liu, C.C. Ling, P.-C. Tao, D.-Z. Pan, Y.-Q. Yang, ZnO single microwire homojunction light-emitting diode grown by electric field assisted chemical vapor deposition, J. Mater. Chem. C 3 (2015) 4678–4682.
[45] S.B. Bashar, M. Suja, M. Morshed, F. Gao, J. Liu, An Sb-doped p-type ZnO nanowire based random laser diode, Nanotechnology 27 (6) (2016), 065204.
[46] I.M. Shafiqul, R. Deep, J. Lin, T. Yoshida, Y. Fujita, Demonstration and evaluation of p-Type and n-Type ZnO nanoparticles-based homojunction UV light-emitting diodes, Phys. Status Solidi RRL 16 (5) (2022) 2100556.
[47] M. Jiang, G. He, H. Chen, Z. Zhang, L. Zheng, C. Shan, D. Shen, X. Fang, Wavelength-tunable electroluminescent light sources from individual Ga-Doped ZnO microwires, Small 13 (19) (2017) 1604034.
[48] X. Zhou, M. Jiang, Y. Wu, K. Ma, Y. Liu, P. Wan, C. Kan, D. Shi, Hybrid quadrupole plasmon induced spectrally pure ultraviolet emission from a single AgNPs@ZnO: Ga microwire based heterojunction diode, Nanoscale Adv. 2 (2020) 1340–1351.
[49] K. Ma, X. Zhou, C. Kan, J. Xu, M. Jiang, Pt nanoparticles utilized as efficient ultraviolet plasmons for enhancing whispering gallery mode lasing of a ZnO microwire via Ga-incorporation, Phys. Chem. Chem. Phys. 23 (2021) 6438–6447.
[50] K. Ma, B. Li, X. Zhou, M. Jiang, Y. Liu, C. Kan, Plasmon-enabled spectrally narrow ultraviolet luminescence device using Pt nanoparticles covered one microwire-based heterojunction, Opt. Express 29 (14) (2021) 21783–21794.
[51] H. Xu, C. Miao, M. Jiang, Y. Liu, C. Kan, D. Shi, Plasmonic enhancement of current-driven whispering gallery polariton device of single microwire based heterojunction via Rh nanocubes deposition, J. Lumin. 235 (2021), 118016.
[52] W. Mao, M. Jiang, J. Ji, P. Wan, X. Zhou, C. Kan, Microcrystal modulated exciton-polariton emissions from single ZnO@ZnO: Ga microwire, Photon. Res. 8 (2) (2020) 175–185.
[53] Y. Sun, M. Jiang, B. Li, X. Xie, C. Shan, D. Shen, Electron-hole plasma Fabry-Perot lasing in a Ga-incorporated ZnO microbelt via Ag nanoparticle deposition, Opt. Express 30 (2) (2022) 740–753.
[54] Y. Liu, M. Jiang, Z. Zhang, B. Li, H. Zhao, C. Shan, D. Shen, Electrically excited hot-electron dominated fluorescent emitters using individual Ga-doped ZnO

microwires via metal quasiparticle film decoration, Nanoscale 10 (2018) 5678–5688.
[55] X. Zhou, M. Jiang, J. Wu, M. Liu, C. Kan, D. Shi, Electrically driven whispering-gallery-mode microlasers in an n-MgO@ZnO: Ga microwire/p-GaN heterojunction, Opt. Express 30 (11) (2022) 18273–18286.
[56] C.X. Xu, F.F. Qin, Q.X. Zhu, J.F. Lu, Y.Y. Wang, J.T. Li, Y. Lin, Q.N. Cui, Z.L. Shi, A. G. Manohari, Plasmon-enhanced ZnO whispering-gallery mode lasing, Nano Res. 11 (6) (2018) 3050–3064.